



# A convenient N<sub>2</sub>–CCl<sub>4</sub> mixture plasma treatment to improve TiO<sub>2</sub> photocatalytic oxidation of aromatic air contaminants under both UV and visible light



Shaozheng Hu\*, Fayun Li, Zhiping Fan

Institute of Eco-environmental Sciences, Liaoning Shihua University, Fushun 113001, PR China

## ARTICLE INFO

### Article history:

Received 23 June 2013

Received in revised form 6 September 2013

Accepted 9 September 2013

Available online 16 September 2013

### Keywords:

N<sub>2</sub>–CCl<sub>4</sub> plasma

TiO<sub>2</sub>

Photocatalysis

Visible light

Chlorine radical

## ABSTRACT

A convenient N<sub>2</sub>–CCl<sub>4</sub> mixture plasma treatment to improve TiO<sub>2</sub> photocatalytic oxidation of aromatic air contaminants under both UV and visible light was reported. X-ray diffraction (XRD), N<sub>2</sub> adsorption, UV-vis spectroscopy, photoluminescence (PL), and X-ray photoelectron spectroscopy (XPS) were used to characterize the prepared TiO<sub>2</sub> catalysts. The microstructures of the TiO<sub>2</sub> catalysts were preserved after plasma treatments. Chlorine ions did not doped into TiO<sub>2</sub> lattice but located on TiO<sub>2</sub> surface via the coordination with Ti<sup>4+</sup> sites. The doping N content of prepared TiO<sub>2</sub> catalyst increased obviously by using this N<sub>2</sub>–CCl<sub>4</sub> mixture plasma method. The activities were tested in the photocatalytic oxidation of benzene and toluene under both UV and visible light. Chlorine radicals which formed under illumination are effective in oxidizing aromatic side groups, but ineffective in reactions with the aromatic ring.

© 2013 Elsevier B.V. All rights reserved.

## 1. Introduction

The heterogeneous photocatalysis of organic and inorganic pollutants both in gas and liquid phase is a significant physicochemical process, thus has been extensively pursued. It is considered to be an effective method to remove several types of air pollutants (NO<sub>x</sub>, SO<sub>2</sub>, volatile organic compounds, etc.) from the atmosphere under UV or visible light radiation. TiO<sub>2</sub> is one of the most promising heterogeneous photocatalysts because of its significant merits, such as optical-electronic properties, low-cost, chemical stability, and non-toxicity [1]. However, there are two aspects limiting its application. The wide band gap nature of titania (3.2 eV for anatase and 3.0 eV for rutile) makes it absorb only ultraviolet (UV) light, which accounts for small fraction of the solar light (3–5%). On the other hand, the high recombination rate of photoexcited electrons and holes make the most of the excitation useless (<90% undergo recombination) [2].

N-doped TiO<sub>2</sub> is the most typical example of the visible-light photocatalysts. Since it was found to be effective under visible light for the decomposition of acetone and methylene blue by Asahi et al. in 2001 [3], N-doping has become a hot topic and been widely investigated. There are large numbers of reports on the states of

N species doped in TiO<sub>2</sub> and the preparation of the photocatalyst by various routes [4–8]. However, the reactivities, stabilities, and quantum efficiencies of visible light responsive N doped TiO<sub>2</sub> catalysts are still in a lower level compared with UV case, thus limiting their practical applications. Besides, it is found sometimes that N doped TiO<sub>2</sub> exhibited lower photocatalytic activity than that of neat TiO<sub>2</sub> under UV light [9]. Therefore, design of more effective and durable photocatalysts under both UV and visible light is still a great challenge in this field.

Recently, halogen modified TiO<sub>2</sub> catalysts attracted more and more attention. Fluorine modification could change the interfacial electron–hole transfer, surface charge distribution, and substrate–surface interaction, thus improve the UV light activity [10,11]. The band gap energy could be narrowed by iodine doping, in a wide range 1.40–2.50 eV, leading to the increased visible light absorption and activity [12–14]. However, only a few literatures reported TiO<sub>2</sub> catalysts modified with chlorine. Xu et al. [15] prepared Cl-doped rutile TiO<sub>2</sub> photocatalyst via a soft interface method, and suggested that the visible light activity was attributed to the narrowed band gap, higher surface acidity, and crystal defects. Wang et al. [16] prepared Cl-doped TiO<sub>2</sub> photocatalyst via a sonication method in water/ethanol system, and found that the band gap energy could be adjusted from 3.2 to 2.2 eV by changing the chlorine concentration. The obtained photocatalyst was used to photodegrade phthalate ester under visible light. Li et al. [17] prepared chlorinated nanocrystalline TiO<sub>2</sub> powders via one-step Ar/O<sub>2</sub> radio frequency thermal plasma oxidizing mists of

\* Corresponding author. Tel.: +86 24 23847473; fax: +86 24 23847473.

E-mail addresses: [hushaozhenglnpu@163.com](mailto:hushaozhenglnpu@163.com), [hushaozheng001@163.com](mailto:hushaozheng001@163.com) (S. Hu).

$\text{TiCl}_3$  solution. The obtained catalyst exhibited narrowed indirect band gaps of 2.65 eV and enhanced UV absorption, thus, showed substantially higher photocatalytic activities than Degussa P25 in the degradation of methyl orange under both visible-light and UV illumination.

Non-thermal plasma is composed of atoms, ions and electrons, which are much more reactive than their molecule precursors. Plasma is able to initiate a lot of reactions, which take place efficiently only at elevated temperatures and high pressures, under mild conditions, thus is used frequently to prepare functional nano-materials. Here, we reported a convenient  $\text{N}_2\text{-CCl}_4$  mixture plasma treatment to improve  $\text{TiO}_2$  photocatalytic activity under both UV and visible light. Combined the results of XRD, UV-vis, and XPS, we confirmed that this method not only doped nitrogen into  $\text{TiO}_2$  crystal lattice, but also located chlorine on the  $\text{TiO}_2$  surface via the coordination with  $\text{Ti}^{4+}$  sites, which narrowed the band gap and increased the quantum efficiency, simultaneously. Benzene and toluene were used as model molecules to investigate the photoactivity of obtained  $\text{TiO}_2$  catalysts. The possible mechanism was proposed.

## 2. Experimental

### 2.1. Preparation and characterization

The doping of  $\text{TiO}_2$  was conducted in a dielectric barrier discharge (DBD) reactor, consisting of a quartz tube and two electrodes. The high-voltage electrode was a stainless-steel rod (2.5 mm), which was installed in the axis of the quartz tube and connected to a high voltage supply. The grounding electrode was an aluminum foil which was wrapped around the quartz tube. For each run, 0.4 g commercial  $\text{TiO}_2$  powder (P25) was charged into the quartz tube.  $\text{N}_2$  from a gas cylinder was allowed to pass through the bed for 3 min to flush out the air. At a constant  $\text{N}_2$  flow ( $20 \text{ ml min}^{-1}$ ), a high voltage of 9–11 kV was supplied by a plasma generator at an overall power input of  $50 \text{ V} \times 0.4 \text{ A}$ . The discharge frequency was fixed at 10 kHz, and the discharge was kept for 6 min. After discharge, the reactor was cooled down to room temperature. The obtained  $\text{TiO}_2$  sample was denoted as PL- $\text{N}_2$ . When the mixture of  $\text{N}_2$  and  $\text{CCl}_4$  vapor (volume ratio = 9:1) was used to replace  $\text{N}_2$  following the same procedure as in the synthesis of PL- $\text{N}_2$ , the obtained product was denoted as PL-mix.

XRD patterns of the prepared  $\text{TiO}_2$  samples were recorded on a Rigaku D/max-2400 instrument using  $\text{Cu-K}\alpha$  radiation ( $\lambda = 1.54 \text{ \AA}$ ). UV-vis spectroscopy measurement was carried out on a Jasco V-550 spectrophotometer, using  $\text{BaSO}_4$  as the reference sample. Nitrogen adsorption was measured at  $-196^\circ\text{C}$  on a Micromeritics 2010 analyzer. All the samples were degassed at 393 K before the measurement. BET Surface area ( $S_{\text{BET}}$ ) was calculated according to the adsorption isotherm. PL spectra were measured at room temperature with a fluorospectrophotometer (FP-6300) using a Xe lamp as excitation source. XPS were conducted on a Thermo Escalab 250 XPS system with  $\text{Al K}\alpha$  radiation as the exciting source. The binding energies were calibrated by referencing the C 1s peak (284.6 eV) to reduce the sample charge effect.

### 2.2. Photocatalytic reaction

Aromatic compounds are an important class of gas pollutants, mainly benzene and toluene. Therefore, toluene and benzene were chosen as the model molecules to evaluate the photocatalytic performance of prepared  $\text{TiO}_2$  catalysts. 0.4 g catalyst was charged into the fixed-bed quartz tube reactor and spread in a thin layer (approximately 1 mm thick). The required quantity of liquid benzene or toluene is injected into the vapor feed reservoir. The obtained gas

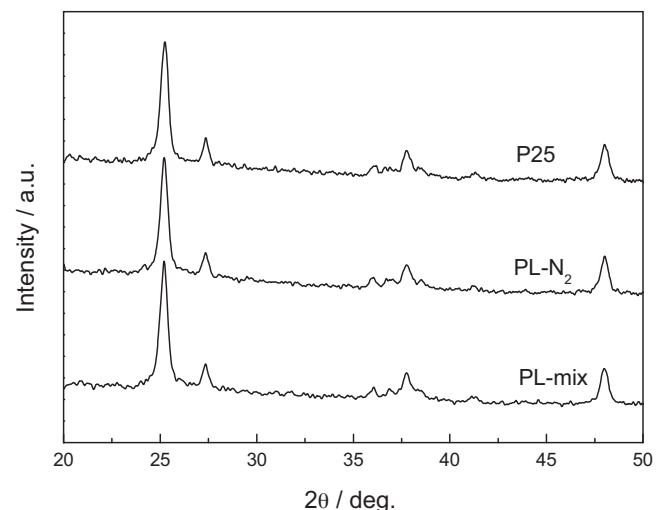


Fig. 1. XRD patterns of P25 and plasma treated samples.

stream which mixed with oxygen (100 ppm) was passed though the reactor with the residence time of 15 s. Prior to the photocatalytic experiment, the catalysts were allowed to reach adsorption equilibrium in the dark. Four 4-W UV lamps with a wavelength centered at 254 nm were placed around the reactor as UV source. In the photoreaction under visible light irradiation, four 500 W Xe lamps with UV cutoff filter ( $\lambda > 420 \text{ nm}$ ) were used. The effluent gas was analyzed using gas chromatograph.

## 3. Results and discussion

It is known that the phase composition and particle size of  $\text{TiO}_2$  have significant influence on its photocatalytic activity. XRD results (Fig. 1) indicated that all peaks can be well indexed to a mixed phase of anatase and rutile present in both P25 and plasma treated catalysts. No N, Cl, and C-derived peak is detected. Thus, plasma treatment does not cause the change in crystallite structure of  $\text{TiO}_2$ . The phase component and the particle sizes of the catalysts were calculated by their XRD patterns according to the method of Spurr and Debye-Scherrer equation respectively [18,19]. The results (Table 1) indicated that there is no obvious change in phase component and particle sizes among three catalysts. Only BET specific surface areas of PL- $\text{N}_2$  and PL-mix decreased slightly compared with P25 powder. From the above analyses, it is revealed that the microstructures of the  $\text{TiO}_2$  were preserved after plasma treatments.

The lattice parameters of the catalysts were measured using (101) and (200) in anatase crystal planes by using equations [20]:

$$d_{(hkl)} = \frac{\lambda}{2 \sin \theta} \quad (1)$$

$$d_{(hkl)}^{-2} = h^2 a^{-2} + k^2 b^{-2} + l^2 c^{-2} \quad (2)$$

where  $d_{(hkl)}$  is the distance between crystal planes of  $(hkl)$ ,  $\lambda$  is the X-ray wavelength,  $\theta$  is the diffraction angle of crystal plane  $(hkl)$ ,  $hkl$  is the crystal index. The  $a$ ,  $b$  and  $c$  are lattice parameters (in anatase form,  $a=b \neq c$ ). The results shown in Table 1 indicated that the lattice parameters of all catalysts remain almost unchanged along  $a$ - and  $b$ -axes, whereas the  $c$ -axis parameter decreased for plasma treated catalysts. This indicated that N atoms doped into the  $\text{TiO}_2$  lattice, leading to the decrease in the cell volume. Besides, it is noted that no obvious difference in lattice parameters were observed between PL-mix and PL- $\text{N}_2$ , indicating Cl and C atoms are not weaved into the crystal structure.

**Table 1**Summary of physical properties of  $\text{TiO}_2$  samples.

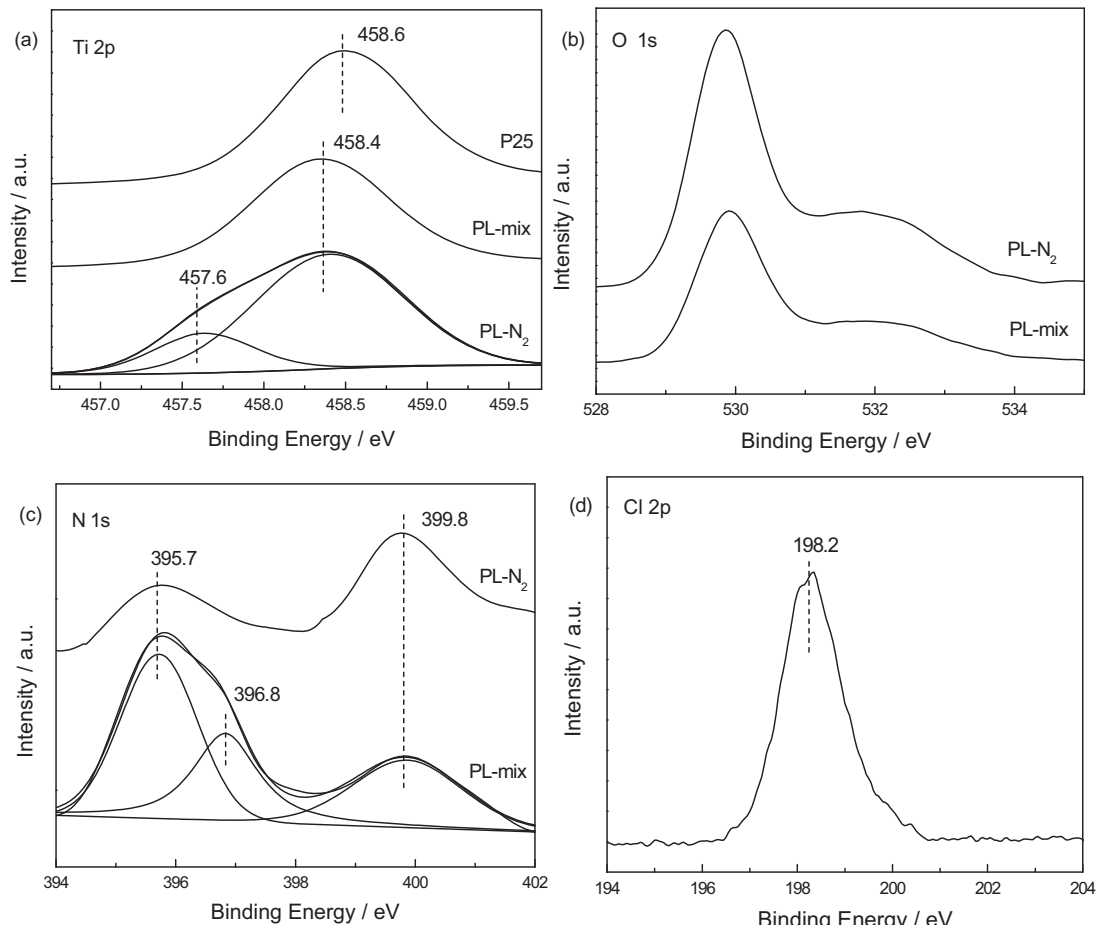
Sample	Size (nm)	<sup>a</sup> $X_A$ (%)	$S_{\text{BET}}$ ( $\text{m}^2/\text{g}$ )	Lattice parameters $a = b, c$ (Å)	$(\text{O} + \text{N})/\text{Ti}$
P25	26.6	76.3	56.3	0.37862, 0.95126	2.0
PL-N <sub>2</sub>	27.3	75.8	54.2	0.37844, 0.94711	1.83
PL-mix	27.1	75.3	53.6	0.37839, 0.94722	1.96

<sup>a</sup>  $X_A$  represents the phase composition of anatase.

XPS has become an increasingly available and powerful tool for understanding the nature of many different types of surfaces. It can provide information about the actual composition and chemical state of surfaces and interfaces that dominate properties of nanosstructured materials. Generally speaking, the binding energy of the element is influenced by its electron density. An increase of binding energy implies the lowering of the electron density. Fig. 2 shows the XP spectra of P25, PL-N<sub>2</sub>, and PL-mix in the region of Ti 2p (a), O 1s (b), N 1s (c), and Cl 2p (d). Compared with P25, obvious shifts to lower binding energy were shown in Ti 2p region for PL-N<sub>2</sub> and PL-mix (Fig. 2a). This is probably attributed to change of chemical environment after N doping [21]. The electrons of N atoms may be partially transferred from N to Ti, due to the higher electronegativity of oxygen, leading to increased electron densities on Ti. For PL-N<sub>2</sub>, the spectra of Ti 2p region were deconvoluted into two contributions, 458.4 and 457.6 eV, which belong to the Ti 2p<sub>3/2</sub> of  $\text{Ti}^{4+}$  and  $\text{Ti}^{3+}$ , respectively [22,23]. This hint  $\text{Ti}^{3+}$  existed in PL-N<sub>2</sub>. In Fig. 2b, the XP spectra of PL-N<sub>2</sub> and PL-mix in O 1s region, the peaks around 530 and 532 eV are attributed to the crystal-lattice oxygen (Ti–O) and surface hydroxyl group (O–H) of  $\text{TiO}_2$ . The ratio of these two peak areas ( $S_{\text{O}-\text{H}}/S_{\text{Ti}-\text{O}}$ ) represents the abundance of surface

hydroxyl groups. The calculation results indicated that  $S_{\text{O}-\text{H}}/S_{\text{Ti}-\text{O}}$  ratio for PL-N<sub>2</sub> was 0.26, much higher than that of PL-mix (0.17). This is probably due to the interaction between  $\text{CCl}_4$  and surface hydroxyl groups under plasma condition. Primet et al. [24] reported that HCl molecules could react with hydroxyl groups on  $\text{TiO}_2$  surface by an ion-exchange reaction. Therefore, in this investigation, it is probably that active chlorine species formed under plasma condition reacted with surface hydroxyl groups to form Ti–Cl bond, leading to the lower hydroxyl groups content.

In Fig. 2c, two common peaks located at 395.7 and 399.8 eV were observed. According to the previous literatures [25,26], those two peaks are attributed to the formation of doping N (Ti–N bond) and other surface N species such as N–N and N–O bond. Besides, another peak located at 396.8 eV was shown for PL-mix, which is probably attributed to the presence of another doping N state in PL-mix. The doping N contents were calculated according to the XPS results and shown in Table 2. Obviously, the doping N content of PL-mix was much higher than that of PL-N<sub>2</sub>. This is possible due to the strong oxophilic ability of  $\text{CCl}_4$ , which is a compound with a high thermodynamical potential of withdrawing oxygen from the lattice host, leading to N doping easier. Besides, the  $N_{\text{doping}}/N_{\text{total}}$

**Fig. 2.** XP spectra of P25, PL-N<sub>2</sub>, and PL-mix in the region of Ti 2p (a), O 1s (b), N 1s (c), and Cl 2p (d).

**Table 2**

Doping N contents in different states of plasma treated samples.

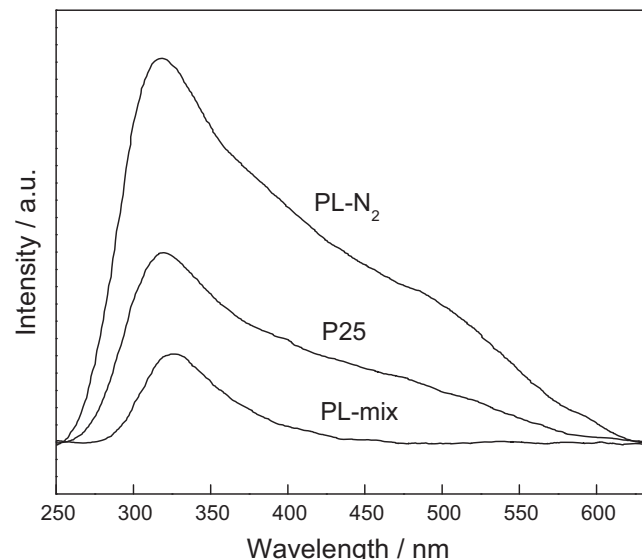
Sample	<sup>a</sup> <i>N</i> <sub>total</sub> (at.%)	<sup>a</sup> <i>N</i> <sub>doping</sub> (at.%)	<i>N</i> <sub>doping</sub> / <i>N</i> <sub>total</sub>
PL-N <sub>2</sub>	1.6	0.5	0.31
PL-mix	2.4	1.6	0.67

<sup>a</sup> *N*<sub>total</sub> and *N*<sub>doping</sub> represent the total and doping N content.

ratio for PL-mix was much higher than that of PL-N<sub>2</sub>. This indicated that N<sub>2</sub>-CCl<sub>4</sub> plasma treatment led to the more favorable formation of the doping N compared with the single N<sub>2</sub> treatment. Besides, the surface (O+N)/Ti ratios were calculated by XP spectra and shown in Table 1. For P25, the (O+N)/Ti ratio was 2.0. For PL-N<sub>2</sub>, this value decreased obviously to 1.83 which was much lower than that of PL-mix (1.96). This indicated that less oxygen vacancies were formed by N<sub>2</sub>-CCl<sub>4</sub> plasma treatment.

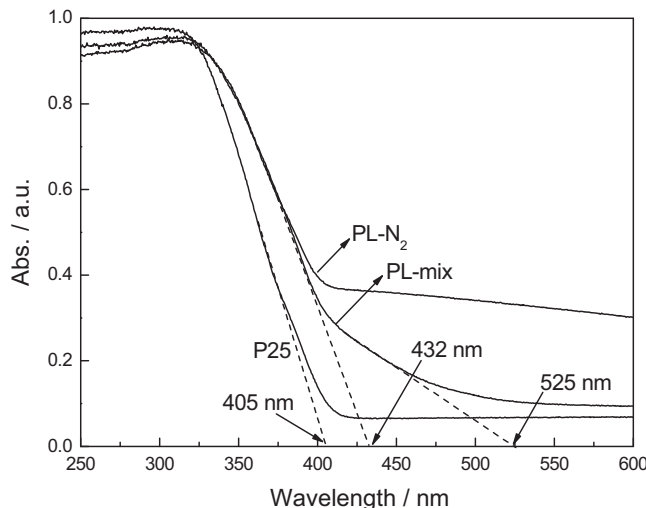
In Fig. 2d, the peak at 198.1 eV was observed for PL-mix. This is very close to that of Cl 2p<sub>3/2</sub> in TiCl<sub>4</sub> (198.2 eV) [27], which is assigned to the chlorine ions linking with the lattice Ti<sup>4+</sup> ions [28,29]. Since the ionic radius of Cl<sup>-</sup> is much larger than that of O<sup>2-</sup> (1.81 Å vs 1.40 Å), lattice oxygen in TiO<sub>2</sub> can hardly be substituted by chlorine ions [27]. No difference in lattice parameters was observed between PL-mix and PL-N<sub>2</sub> confirmed this point of view. Thus, it is concluded that the chlorine ions located on the TiO<sub>2</sub> surface via the coordination with Ti<sup>4+</sup> sites. The chlorine content on TiO<sub>2</sub> surface was 0.6 at.% calculated by XP spectra data.

Usually, N doping obviously affects light absorption characteristics of TiO<sub>2</sub>. UV-vis spectra of prepared TiO<sub>2</sub> catalysts are shown in Fig. 3. Bare TiO<sub>2</sub> (P25) was not able to respond to visible light, whereas two plasma treated catalysts extended the absorption edges to visible light region, which must result from nitrogen doped into TiO<sub>2</sub> lattice. In order to calculate the onsets of absorption edges, a tangent was drawn on absorption spectra and was extrapolated. The intercept on the wavelength axis was obtained. The results showed that the absorption edges for P25 and PL-N<sub>2</sub> were 405 and 432 nm. Whereas, for PL-mix, two absorption edges were observed, 432 and 525 nm. The band gaps of the TiO<sub>2</sub> catalysts were calculated according the method of Oregan et al. [30]. The results shown in Table 1 indicated that the band gaps for P25 and PL-N<sub>2</sub> were 3.06 and 2.87 eV. For PL-mix, two band gaps, 2.87 and 2.36 eV were observed. It is proved that chlorine ions did not doped into the TiO<sub>2</sub> lattice but locate on the TiO<sub>2</sub> surface via the coordination with Ti<sup>4+</sup> sites. Therefore, those narrowed band gaps were not attributed to the chlorine doping. Di Valentin et al. [31] provided

**Fig. 4.** PL spectra of P25, PL-N<sub>2</sub>, and PL-mix.

theoretical evidence that for substitutional N doped TiO<sub>2</sub>, the visible light response arises from occupied N 2p localized states slightly above the valence band edge (0.14 eV), whereas for interstitial N-doped TiO<sub>2</sub>, the visible light response arises from occupied π\* character N–O localized states above the valence band edge (0.73 eV). These theoretical data were quite consistent with our experimental results. XPS result confirmed the presence of another doping N state in PL-mix. Therefore, in this work, it is concluded that the substitutional N present in PL-N<sub>2</sub>, whereas substitutional and interstitial N existed in PL-mix simultaneously. Besides, for PL-N<sub>2</sub>, a broad absorption over 400 nm is observed. Huang et al. [32] prepared the visible light responsive TiO<sub>2</sub> by nitrogen-plasma surface treatment, and found the similar broad absorption in visible light region. Such broad absorption originated probably from the superposition of d–d transitions in Ti<sup>3+</sup> species and oxygen vacancies [33]. This confirmed the oxygen vacancies content of PL-N<sub>2</sub> was higher than that of PL-mix.

During the recombination process of photo-induced charge carriers, a certain amount of chemical energy can be released, which would further transform possibly to heat or to light energy. The light energy can be dissipated as radiation, which results in a luminescence emission of semiconductor material, called the PL phenomenon of the semiconductor. PL is a highly sensitive technique used to investigate the photophysical and photochemical properties of solid semiconductors, and can provide information on charge separation/recombination of photoinduced charged carriers (electron/hole), as well as surface defects [34,35]. In general, the lower the PL intensity, the lower the recombination rate of photo-induced electron–hole pairs, thus the higher the photocatalytic activity. Fig. 4 shows the PL spectra of P25 and plasma treated TiO<sub>2</sub> samples. Two main peaks which located around 330 and 500 nm were observed. According to the previous report, the peak located around 330 is mainly ascribed to the band–band PL signal, whereas the other peak at around 500 nm was attributed to the excitonic PL, which mainly resulted from surface oxygen vacancies and defects [36,37]. For PL-N<sub>2</sub>, the peak intensity around 500 nm was much higher than that of other two catalysts, indicating more surface oxygen vacancies and defects existed which played the role of recombination center. Besides, Ollis et al. [38,39] reported that the surface-bound chloride groups could be converted to chlorine radicals by trapping photogenerated holes if being irradiated by UV light. Therefore, compared with P25, the lower PL intensity of PL-mix should be attributed to the decreased electrons/holes

**Fig. 3.** UV-vis spectra of P25, PL-N<sub>2</sub>, and PL-mix.

**Table 3**

The formation heat data of compounds.

Compound	$\text{OH}^{\bullet}$	$\text{Cl}^{\bullet}$	$\text{C}_6\text{H}_6$	$\text{C}_6\text{H}_5\text{CH}_3$	$\text{HOH}$	$\text{HCl}$	$\text{C}_6\text{H}_5^{\bullet}$	$\text{C}_6\text{H}_5\text{CH}_2^{\bullet}$
$\Delta H_{\text{form}}/\text{kJ mol}^{-1}$	38.9	121.7	82.9	50.0	-241.8	-92.3	329	200

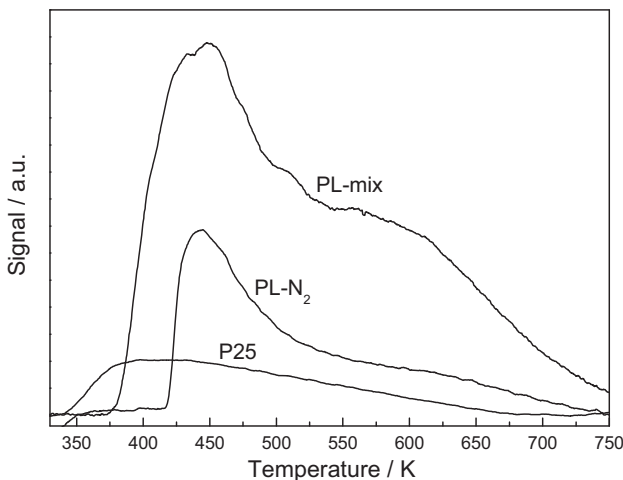


Fig. 5.  $\text{NH}_3$ -TPD profiles of P25, PL- $\text{N}_2$ , and PL-mix.

recombination caused by surface-bound chloride groups, thus leading to the increased quantum efficiency. Besides, for PL-mix, N doping causes the decreased cell volume because of the difference in atomic radius (Table 1). The interactions between different atoms lead to the bond length will also change. These changes of the cell volume and bond length result in the distortion of  $\text{TiO}_6$  octahedron. The more doping N content, the more distortion occurred. Such distorted  $\text{TiO}_6$  octahedron lead to the formation of dipole moment, which also favors the separation of photoexcited electron-hole pairs [4].

$\text{NH}_3$ -TPD was used to investigate the surface acid of  $\text{TiO}_2$  catalysts, and shown in Fig. 5. Low  $\text{NH}_3$  desorption peaks were observed for P25 and PL- $\text{N}_2$ , whereas a broad desorption peaks in the temperature range 390–780 K with two peak maxima at 460 and 570 K were observed for  $\text{N}_2-\text{CCl}_4$  plasma treated catalyst, PL-mix. According to previous reports, these two peaks were normally attributed to  $\text{NH}_3$  chemisorbed to weak and strong acid sites, respectively [40,41]. Xu et al. [15] prepared the Cl doped rutile  $\text{TiO}_2$ , measured the surface acidity by  $^1\text{H}$  MAS NMR, and suggested that as-prepared Cl– $\text{TiO}_2$  demonstrated a stronger acidity than P25. Therefore, such increased surface acid sites on plasma treated catalysts should be related to the high electronegativity of chlorine, leading to the adjacent titanium atom more “positively charged”, which could play the role as Lewis acidic sites. These sites are more favorable to interact with the  $\pi$  electrons of aromatic ring, leading to the increased adsorption capacity of benzene and toluene which is favorable to the photocatalytic reaction.

Fig. 6 shows the photocatalytic degradation of toluene and benzene over P25, PL- $\text{N}_2$ , and PL-mix under both UV and visible light irradiation. It is shown that all the catalysts exhibited stable activities during the photocatalytic degradation reaction. Under UV light, the toluene and benzene conversions decreased in the order: PL-mix > P25 > PL- $\text{N}_2$  (Fig. 6a and c), which is opposite to the PL intensity order (Fig. 4). This indicated that the quantum efficiency plays a significant important role on the UV light activity. Under visible light, P25 had no photocatalytic activity for the degradation of toluene and benzene. Whereas, after plasma treatment, PL- $\text{N}_2$  exhibited improved toluene and benzene conversion. Since the microstructures of the  $\text{TiO}_2$  catalysts were preserved

**Table 4**

Calculated heats of reaction for hydrogen abstraction from benzene and toluene.

Reaction	$\Delta H/\text{kJ mol}^{-1}$
$\text{OH}^{\bullet} + \text{C}_6\text{H}_6 \rightarrow \text{HOH} + \text{C}_6\text{H}_5^{\bullet}$	-34.8
$\text{OH}^{\bullet} + \text{C}_6\text{H}_5\text{CH}_3 \rightarrow \text{HOH} + \text{C}_6\text{H}_5\text{CH}_2^{\bullet}$	-130.8
$\text{Cl}^{\bullet} + \text{C}_6\text{H}_6 \rightarrow \text{HCl} + \text{C}_6\text{H}_5^{\bullet}$	31.9
$\text{Cl}^{\bullet} + \text{C}_6\text{H}_5\text{CH}_3 \rightarrow \text{HCl} + \text{C}_6\text{H}_5\text{CH}_2^{\bullet}$	-64

after plasma treatments, the enhanced photocatalytic activity must result from the doping of nitrogen in  $\text{TiO}_2$ , which gave rise to the narrowed band gap and thus to the enhanced absorption in the visible region. It is noted that the benzene conversion was lower than that of toluene over plasma treated catalysts under both UV and visible light. This is probably due to that benzene has a very stable aromatic structure and is less susceptible to photocatalytic oxidation.

Ollis et al. [38,39] reported that chlorine radicals are less energetic than hydroxyl radicals, which could be formed even under visible light irradiation. Moreover, the chlorine radicals can attack organic substances having weakly bound branch hydrogen (such as propylene and toluene) and effectively destruct them into inorganic small molecules by a chain transfer oxidation that is faster than the corresponding reaction with hydroxyl radicals [38,39]. Thus, the toluene conversion over PL-mix was much higher than that of PL- $\text{N}_2$  under visible light (Fig. 6b). Besides, the lower band gap energy and electron/hole recombination rate of PL-mix, which proved by UV-vis and PL spectra, caused the more efficient utilization of visible light and the better quantum efficiency, thus increased the toluene conversion. However, in Fig. 6d, the benzene conversion over PL-mix was lower than that of PL- $\text{N}_2$  under visible light. It should be possible that the holes and hydroxyl radicals are highly reactive in photocatalysis, especially for the cleavage of aromatic rings [42,43], whereas chlorine radicals are less energetic than hydroxyl radicals, thus it is difficult to oxidize benzene by chlorine radicals directly under visible light. The consuming of the holes for the generation of chlorine radicals will certainly decrease the proportion of the total number of holes that could be converted into hydroxyl radicals, thus leading to the decreased benzene conversion. Only when the PL-mix was excited by UV light, with a higher energy, more photogenerated holes and electrons produced. Accordingly, the holes were substantially available for the formation of hydroxyl radicals, and the chlorine radical can attack the formed intermediates undergoing cleavage reactions, resulting in the higher conversions of toluene and benzene over PL-mix (Fig. 6a and c).

To confirm the discussion above, the theoretical calculations are provided. Table 3 shows the formation heat data of compounds [44]. Using these formation heat data, corresponding heats of reaction,  $\Delta H$ , for hydrogen abstraction reactions from benzene and toluene are calculated (Table 4). Obviously, hydrogen abstraction reactions involving photocatalytically generated hydroxyl radicals are thermodynamically feasible ( $\Delta H$  is negative), for the removal of both methyl group hydrogen on toluene and aromatic ring hydrogen on benzene. Abstraction of methyl group hydrogen is also thermodynamically more favorable than abstraction of ring hydrogens. These thermodynamic predictions are consistent with our experimental results, in which both benzene and toluene are subject to photocatalytic degradation, moreover benzene displays lower removal rates than toluene. The thermodynamic predictions for the action of

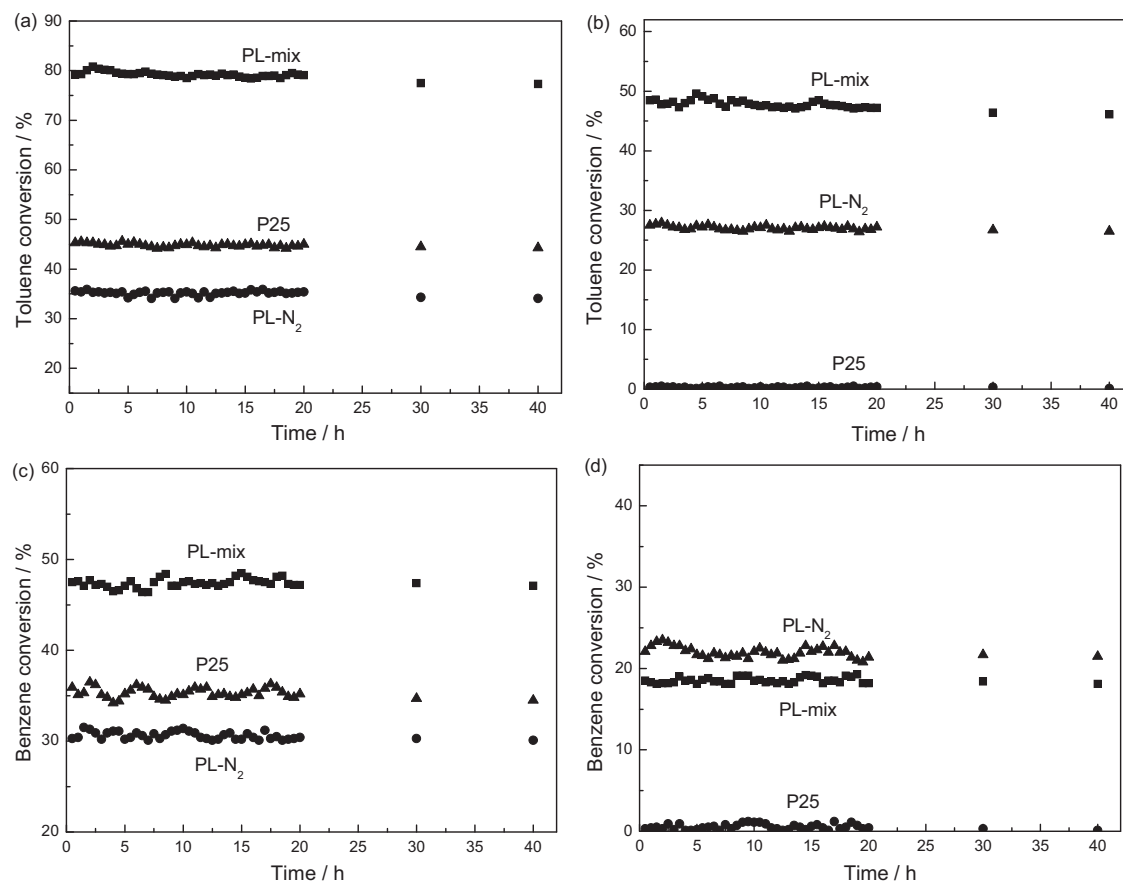


**Fig. 6.** Photocatalytic activity of P25, PL-N<sub>2</sub>, and PL-mix: toluene conversion under UV (a) and visible (b) light irradiation; benzene conversion under UV (c) and visible (d) light irradiation.

chlorine radicals indicated that the removal of methyl group hydrogen on toluene is thermodynamically feasible, whereas the removal of aromatic ring hydrogen on benzene is not feasible ( $\Delta H$  is positive). Thus the toluene conversion over PL-mix was higher than that of PL-N<sub>2</sub>, whereas benzene conversion over PL-mix was lower than that of PL-N<sub>2</sub> under visible light (Fig. 6b and d).

After 40 h reaction, the catalyst PL-mix was collected and measured by XP spectra. The content of doping N and chlorine only decreased slightly compared with fresh PL-mix (1.4 and 0.5 at.% to 1.6 and 0.6 at.%), indicating the good stability of catalyst. According to the above conclusions, a possible mechanism for the performance enhancement in PL-mix catalyst was proposed. Under UV or visible light irradiation, electrons and holes were generated, and reacted with adsorbed O<sub>2</sub> and surface hydroxyl group to form •O<sub>2</sub><sup>-</sup> and •OH radicals, which directly oxidized the model molecules [2]. Besides, surface-bound chloride groups could be converted to chlorine radicals by trapping photogenerated holes. The formed chlorine radicals can abstract methyl group hydrogen on toluene to form HCl and activated C<sub>6</sub>H<sub>5</sub>CH<sub>2</sub><sup>•</sup> species, which is faster than the corresponding reaction with hydroxyl radicals. Then C<sub>6</sub>H<sub>5</sub>CH<sub>2</sub><sup>•</sup> species could be oxidized by O<sub>2</sub> completely to form CO<sub>2</sub> and H<sub>2</sub>O. On the other hand, chlorine radicals cannot abstract the ring hydrogens of benzene. But •O<sub>2</sub><sup>-</sup> and •OH radicals can oxidize the benzene to form the intermediates with weakly bound branch hydrogen. Such intermediates could be oxidized by the chlorine radicals, thus improved the benzene conversion under UV light. In addition, H<sub>2</sub>O was one of the final products in the photocatalytic reaction and could be adsorbed and converted into surface hydroxyl groups [45]. As a result, the formed HCl molecules rechemisorbed and

circulated to form surface Ti–Cl groups under irradiation [24], resulting in good stability.

#### 4. Conclusion

A convenient N<sub>2</sub>–CCl<sub>4</sub> mixture plasma treatment to improve TiO<sub>2</sub> photocatalytic activity under both UV and visible light was reported. The microstructures of the TiO<sub>2</sub> catalysts were preserved after plasma treatments. Chlorine ions did not dope into TiO<sub>2</sub> lattice but located on the TiO<sub>2</sub> surface via the coordination with Ti<sup>4+</sup> sites. Toluene conversion over PL-mix was much higher than that of PL-N<sub>2</sub> under both UV and visible light. This is due to that chlorine radicals are less energetic than hydroxyl radicals, which could be formed even under visible light irradiation. The formed chlorine radicals can attack methyl group hydrogen on toluene and effectively destruct them into inorganic small molecules by a chain transfer oxidation that is faster than the corresponding reaction with hydroxyl radicals. However, the benzene conversion over PL-mix was lower than that of PL-N<sub>2</sub> under visible light. This is due to that chlorine radicals are less energetic than hydroxyl radicals, thus removal of aromatic ring hydrogen with higher energy is difficult by chlorine radicals directly under visible light.

#### Acknowledgments

This work was supported by National Natural Science Foundation of China (Nos. 41071317, 30972418), National Key Technology R & D Program of China (Nos. 2007BAC16B07, 2012ZX07505-001),

and the Natural Science Foundation of Liaoning Province (No. 20092080).

## References

- [1] M.R. Hoffmann, S.T. Martin, W. Choi, D.W. Bahnemann, *Chem. Rev.* 95 (1995) 69–96.
- [2] X.D. Wang, R.A. Caruso, *J. Mater. Chem.* 21 (2011) 20–28.
- [3] R. Asahi, T. Morikawa, T. Ohwaki, A. Aoki, Y. Taga, *Science* 293 (2001) 269–271.
- [4] M. Sathish, B. Viswanathan, R.P. Viswanath, C.S. Gopinath, *Chem. Mater.* 17 (2005) 6349–6354.
- [5] J.L. Gole, J.D. Stout, C. Burda, Y. Lou, X. Chen, *J. Phys. Chem. B* 108 (2004) 1230–1240.
- [6] S. Sato, R. Nakamura, S. Abe, *Appl. Catal. A: Gen.* 284 (2005) 131–137.
- [7] E.A. Reyes-Garcia, Y. Sun, K. Reyes-Gil, D. Raftery, *J. Phys. Chem. C* 111 (2007) 2738–2748.
- [8] X.C. Wang, J.C. Yu, Y.L. Chen, L. Wu, X.Z. Fu, *Environ. Sci. Technol.* 40 (2006) 2369–2374.
- [9] S.Z. Hu, F.Y. Li, Z.P. Fan, C.C. Chang, *Appl. Surf. Sci.* 258 (2011) 182–188.
- [10] M.S. Vohra, S. Kim, W. Choi, *J. Photochem. Photobiol. A: Chem.* 160 (2003) 55–60.
- [11] H. Kim, W. Choi, *Appl. Catal. B: Environ.* 69 (2007) 127–132.
- [12] X.T. Hong, Z.P. Wang, W.M. Cai, F. Lu, J. Zhang, Y.Z. Yang, N. Ma, Y.J. Liu, *Chem. Mater.* 17 (2005) 1548–1552.
- [13] G. Liu, Z.G. Chen, C.L. Dong, Y.N. Zhao, F. Li, G.Q. Lu, H.M. Cheng, *J. Phys. Chem. B* 110 (2006) 20823–20828.
- [14] S. Tojo, T. Tachikawa, M. Fujitsuka, T. Majima, *J. Phys. Chem. C* 112 (2008) 14948–14954.
- [15] H. Xu, Z. Zheng, L. Zhang, H. Zhang, F. Deng, *J. Solid State Chem.* 181 (2008) 2516–2522.
- [16] X.K. Wang, C. Wang, W.Q. Jiang, W.L. Guo, J.G. Wang, *Chem. Eng. J.* 189/190 (2012) 288–294.
- [17] J.G. Li, M. Ikeda, C. Tang, Y. Moriyoshi, H. Hamanaka, T. Ishigaki, *J. Phys. Chem. C* 111 (2007) 18018–18024.
- [18] R.A. Spurr, H. Myers, *Anal. Chem.* 29 (1957) 760–762.
- [19] J. Lin, Y. Lin, P. Liu, M.J. Meziani, L.F. Allard, Y.P. Sun, *J. Am. Chem. Soc.* 124 (2002) 11514–11518.
- [20] X.Z. Shen, Z.C. Liu, S.M. Xie, J. Guo, *J. Hazard. Mater.* 162 (2009) 1193–1198.
- [21] H.X. Li, J.X. Li, Y.N. Huo, *J. Phys. Chem. B* 110 (2006) 1559–1565.
- [22] S.Z. Chen, P.Y. Zhang, W.P. Zhu, L. Chen, S.M. Xu, *Appl. Surf. Sci.* 252 (2006) 7532–7538.
- [23] F. Peng, L.F. Cai, H. Yu, H.J. Wang, J. Yang, *J. Solid State Chem.* 181 (2008) 130–136.
- [24] M. Primet, J. Basset, M.V. Matthieu, M. Prettre, *J. Phys. Chem.* 74 (1970) 2868–2874.
- [25] K. Yamada, H. Yamane, S. Matsushima, H. Nakamura, K. Ohira, M. Kouya, K. Kumada, *Thin Solid Films* 516 (2008) 7482–7487.
- [26] K. Yamada, H. Yamane, S. Matsushima, H. Nakamura, T. Sonoda, S. Miura, K. Kumada, *Thin Solid Films* 516 (2008) 7560–7564.
- [27] J. Wang, W. Wu, D. Feng, *The Introduction of Electronic Spectroscopy*, The Publishing House of Defense Industry, Beijing, 1992.
- [28] E. Wang, W. Yang, Y. Cao, *J. Phys. Chem. C* 113 (2009) 20912–20917.
- [29] J. Zhu, W. Zheng, B. He, J. Zhang, M. Anpo, *J. Mol. Catal. A* 216 (2004) 35–43.
- [30] B. Oregan, M. Gratzel, *Nature* 353 (1991) 737–740.
- [31] C. Di Valentini, G. Pacchioni, A. Selloni, S. Livraghi, E. Giamello, *J. Phys. Chem. B* 109 (2005) 11414–11419.
- [32] C.M. Huang, L.C. Chen, K.W. Cheng, G.T. Pan, *J. Mol. Catal. A* 261 (2007) 218–224.
- [33] A.V. Emeline, N.V. Sheremeteva, N.V. Khomchenko, V.K. Ryabchuk, N. Serpone, *J. Phys. Chem. C* 111 (2007) 11456–11462.
- [34] H. Nakajima, T. Mori, Q. Shen, T. Toyoda, *Chem. Phys. Lett.* 409 (2005) 81–84.
- [35] J.Y. Shi, J. Chen, Z.C. Feng, T. Chen, Y.X. Lian, X.L. Wang, C. Li, *J. Phys. Chem. C* 111 (2007) 693–699.
- [36] J. Yu, L. Yue, S. Liu, B. Huang, X. Zhang, *J. Colloid Interface Sci.* 334 (2009) 58–64.
- [37] L.Q. Jing, Y.C. Qu, B.Q. Wang, S.D. Li, B.J. Jiang, L.B. Yang, W. Fu, H.G. Fu, J.Z. Sun, *Sol. Energy Mater. Sol. Cells* 90 (2006) 1773–1787.
- [38] Y. Luo, D.F. Ollis, *J. Catal.* 163 (1996) 1–11.
- [39] O. d'Hennezel, D.F. Ollis, *J. Catal.* 167 (1997) 118–126.
- [40] D. Li, H. Haneda, S. Hishita, N. Ohashi, *Chem. Mater.* 17 (2005) 2588–2595.
- [41] D. Li, N. Ohashi, S. Hishita, T. Kolodiaznyi, H. Haneda, *J. Solid State Chem.* 178 (2005) 3293–3302.
- [42] X. Fu, W.A. Zeltner, M.A. Anderson, *Appl. Catal. B: Environ.* 6 (1995) 209–224.
- [43] D.S. Bhatkhande, V.G. Pangarkar, A. Beenackers, *ACM J. Chem. Technol. Biotechnol.* 77 (2002) 102–116.
- [44] R.C. Weast (Ed.), *CRC Handbook of Chemistry and Physics*, 1st Student ed., CRC Press, Boca Raton, FL, 1988.
- [45] X. Wang, J.C. Yu, P. Liu, X. Wang, W. Su, X. Fu, *J. Photochem. Photobiol. A: Chem.* 179 (2006) 339–347.